Supplementary Information

Supplementary Note 1: Kinetic Model of QS-based Dynamic Switching at the G6P Branchpoint

Dynamic Mass Balances on Metabolites

The model for dynamic knockdown of Pfk-1 was adapted from Brockman et al[1] and implemented in MATLAB. The structure of the model was centered around the glucose-6-phosphate (G6P) branchpoint shared by glycolysis (Pgi and Pfk-1) and the glucaric acid pathway (INO1) in a strain in which *zwf* has been deleted. Kinetic parameters for enzymes included in the model are given in Supplementary Table 4, as are the kinetic equations utilized. Enzyme kinetics for these four reactions were based on standard Michaelis-Menten forms for reversible and irreversible enzyme reactions, as suggested in Chassagnole et al[2] and summarized below:

Irreversible two substrate Michaelis-Menten:

$$v = \upsilon_{max} E \frac{S_1 S_2}{K_{iS_1} K_{MS_2} + K_{MS_1} S_2 + K_{MS_2} S_1 + S_1 S_2}$$

Reversible Michaelis-Menten:

$$v = \upsilon_{max} E \frac{S_1 - \frac{S_2}{K_{eq}}}{S_1 + K_{MS_1}\left(1 + \frac{S_2}{K_{MS_2}}\right)}$$

where S1 and S2 are the respective substrates and E is the enzyme level (scaled to 1 for wild-type levels of enzyme). K_{iS_1} is the equilibrium dissociation constant of S1, but was set equal to K_{MS_1}, as in the irreversible two-substrate Michaelis-Menten equations used in Chassagnole et. al[2]. Values for steady-state G6P and fructose-6-phosphate (F6P) levels, cofactor pools, and glucose uptake rate were taken from Chassagnole et al[2] and were used to calculate the υ_{max} for each enzyme. Further, the υ_{max} for INO1 was calculated based on activity measurements in crude cell lysates and total protein levels[3].

These calculated υ_{max} values were then utilized in the mass balances of G6P and F6P, as summarized below, to calculate the dynamic profile of these metabolites, such as when Pfk-1 levels were knocked down.

$$\frac{dG6P}{dt} = v_{pts} - v_{pgi} - v_{ino1} - F_{Pfk}\,\mu\,G6P$$

$$\frac{dF6P}{dt} = v_{pgi} - v_{Pfk} - F_{Pfk}\,\mu\,F6P$$

F_{Pfk} denotes the fractional Pfk-1 activity at a given time, with the maximum being 1 when there is no Pfk-1 knockdown. μ represents growth rate of the culture.

Autonomous Knockdown of Pfk-1 from QS-based AHL buildup

A mass action kinetics-based approach for production and degradation of AHL was used, as implemented in previous quorum sensing models[4]. Further, a standard carrying capacity model was utilized to describe the biomass profile in the culture. As a first order approximation, the effect of different Pfk-1 activity levels on growth rate and final biomass was assumed to be linear. Moreover, the expression of Pfk-1 (and F_{Pfk}) is knocked down based on the buildup of AHL. The mathematical structure of the effect of AHL on F_{Pfk}, and the cumulative dissociation constant (K_d), are taken from Shong et al[5] which showed that the cumulative response of EsaR-regulated promoters was non-cooperative with respect to AHL concentration, and can be modeled as a standard repression response with a Hill coefficient of 1. The equations summarizing QS-based culture dynamics are summarized as follows:

Cellular growth:

$$\frac{dN}{dt} = F_{Pfk}\mu N(1 - \frac{N}{F_{Pfk}N_m})$$

AHL balance:

$$\frac{dAHL}{dt} = k_{AHL}N - d_{AHL}A$$

Fractional Pfk-1 activity:

$$\frac{dF_{Pfk}}{dt} = \left(-\frac{K_d}{(K_d + AHL)^2}\right) * (k_{AHL}N - d_{AHL}A)$$

where k_{AHL} and d_{AHL} are the production and degradation rates of AHL, respectively, as presented in You et al[4]. The maximum biomass value, N_m, was set to 10^9 cells/mL to correspond approximately to the expected biomass when fed 10 g/L glucose in minimal media. As biomass increases, it leads to greater AHL production and decline in fractional Pfk-1 activity. This feeds back to decrease the growth rate. As F_{Pfk} decreases over time, the steady state pools of G6P and F6P increase, thereby increasing the flux through INO1 over the course of the run. The flux through INO1 can be integrated over time and scaled by the biomass profile in the culture to give a prediction of the total MI titers at the end of the fermentation. This model was constructed to provide a basis for qualitative trends expected from experimental implementation of dynamic regulation for MI production. Further measurements and parameter characterization can be performed to make the model precisely predictive. Model results are given in Supplementary Figure 1.

Supplementary Note 2: Phosphate starvation to induce gene expression and Pfk-1 knockdown

A previous configuration for dynamic downregulation of Pfk-1 activity relied upon the appendage of an SspB-dependent SsrA tag, and required manual addition of inducers to initiate production of SspB to recruit ClpXP to the tagged protein and trigger active degradation[1]. In this new architecture, the promoter driving *sspB* expression in the genome was replaced with one that is activated upon depletion of phosphate (P_{phoA})[6] to allow autonomous induction of *sspB* and post-translational knockdown of Pfk-1 activity in a *zwf* knockout strain upon phosphate depletion (Supplementary Fig. 11A). The *pfkA* sequence was appended to an SspB-dependent degradation tag (AADENYSENYADAS, "DAS+4")[7], and was inserted in the genome under a constitutive promoter from the BioFAB registry (apFAB114 or apFAB104), yielding strains IB643 and IB1509 (Supplementary Table 2). In MOPS minimal medium with glucose as the sole carbon source, depletion of phosphate led to induction of *sspB*, resulting in rapid degradation of Pfk-1 protein in the cell, arrest of cell growth and redirection of flux into MI production. This was compared against a strain where *sspB* expression was driven by an aTc-inducible promoter (IB1863, Supplementary Table 2), but was not induced.

Upon phosphate starvation, IB1863 showed no decrease in Pfk-1 activity, while both IB643 and IB1509 showed decreases (Supplementary Fig. 11B). The baseline activity under excess phosphate revealed that IB643 had a much lower basal Pfk-1 activity than either IB1863 or IB1509. Thus, we decided to proceed with IB1509 for MI production as it more closely matched the control. Both strains showed a boost in titers in phosphate-limiting conditions (Supplementary Fig. 11C) if growth was arrested at an intermediate point with phosphate depletion. With initial phosphate levels too low (highly phosphate-limited), sufficient biomass could not be formed and glucose was not fully depleted. Thus, a higher phosphate concentration (0.2 g/L) still allowed phosphate depletion in the culture at a later time while allowing more biomass to build up. Interestingly, we observed that even in the IB1863 control, a boost in MI titers was observed under phosphate-limiting conditions and was not discernible from that obtained from IB1509 (Supplementary Fig. 11C). The reasons for this have not yet been fully investigated, but could include natural limitation of glycolytic flux during phosphate starvation or upregulation of endogenous phosphatases that dephosphorylate *myo*-inositol-1-phosphate to MI more rapidly, helping to pull flux through INO1.

The use of phosphate starvation to drive *sspB* expression, and correspondingly drive a reduction in Pfk-1 activity, is an interesting strategy for a number of reasons. Phosphate is an essential nutrient and phosphate starvation strategies have already been demonstrated to improve yields for a number of products, such as shikimic acid and fatty acids[8,9]. Additionally, phosphate feeding could be used to achieve cycling in the Pfk-1 activity level, unlike in the case of inducer addition, where once added, the inducer cannot be easily removed to stop *sspB* expression and allow recovery of Pfk-1 activity. However, nutrient starvation also induces a wide variety of regulatory responses in the cell, some of which may be undesirable for product formation. Furthermore, linking nutrient starvation with a specific, desired outcome could provide a route to enhance positive effects on production, but it may still be difficult to achieve general applicability for different pathways and products, as seen by our results above. This strategy also relies specifically on the medium composition, such that a precise amount of phosphate must be present in order to enable switching at desired times. This may be especially undesirable for industrial production where media formulations may be tailored to the pathway and products of interest or may include complex feedstocks and other

components for more economical process operation[10,11]. This limitation extends to all nutrient-based strategies as they rely on the careful manipulation and monitoring of medium recipes.

Supplementary Note 3: Quorum sensing-based post-translational knockdown of Pfk-1

The EsaR-repression architecture was utilized to induce post-translational degradation of cellular Pfk-1 protein (Supplementary Fig. 13). Specifically, the *pfkA* sequence in the genome was appended to a modified SsrA tag (AADENYSENYADAS, "DAS+4")[7] that induces rapid protein degradation in the presence of SspB, a protein that recruits ClpXP to the tagged site. This tagged *pfkA* was inserted into its native locus under the control of a constitutive promoter from the BioFAB registry (apFAB114). An *esaR*-P_{esaR}-*ssp*B cassette was separately integrated into the genome in which *esaR* was driven by a constitutive BioFAB promoter (apFAB104), while *sspB* was under the control of the P_{esaR} promoter. Flux into the pentose phosphate pathway was arrested by knocking out *zwf*, yielding strain IB2265 (Supplementary Table 2). In the absence of AHL, EsaR is bound to the P_{esaR} promoter and prevents production of SspB. The control IB1643 strain, which contained tagged *pfkA* under the same promoter as IB2265 but with no *esaR*-P_{esaR}-*sspB* expression cassette, exhibited no decline in Pfk-1 activity with or without AHL (Supplementary Fig. 14A). On the other hand, IB2265 exhibited low Pfk-1 activity, even in the absence of any AHL. Exogenous addition of AHL led to no further decline in activity, suggesting that SspB may already be present due to leaky expression from the P_{esaR} promoter. Furthermore, in minimal medium with glucose as the sole carbon source, this strain exhibited no growth in the presence or absence of AHL (Supplementary Fig. 14B).

In order to reduce basal leaky expression of *sspB*, the strength of the RBS controlling its translation was tuned down directly within the genome through insertion of a degenerate base-pair library and Cas9-based counterselection[12,13]. This led to a spectrum of strains containing RBS variants of different strengths. Colonies were screened for growth on MOPS minimal medium with glucose as the sole carbon source, in the presence and absence of exogenously added AHL using the BioLector microbioreactor system. Several colonies were isolated that showed normal and no growth in the absence and presence of added AHL, respectively (Supplementary Fig. 14B). One was then chosen that had the weakest predicted RBS strength (AG2349) and was used for further characterization and production trials.

esaI was genomically-integrated into AG2349 under the control of the EsaI promoter-RBS library to yield a spectrum of AHL production rates. As AHL is constitutively produced, its buildup leads EsaR to unbind from P_{esaR} and allow SspB production, resulting in growth arrest in minimal medium with glucose. Only the weakest two EsaI expression cassettes (L25R and L31R) allowed strains to grow measurably before leading to growth arrest (Supplementary Table 2). These were transformed with the pTrc-INO1 plasmid[3] to enable MI production. MI titers showed no improvement from L25R or L31R over wildtype IB1379 (Supplementary Fig. 14C). Pfk-1 activity profiles still showed a decline in activity in AG2349 despite the absence of EsaI in this strain, indicating there was still notable leaky activity of SspB (Supplementary Fig. 14D).

While this system was unsuitable for controlling degradation of Pfk-1 through *sspB* induction, it may still be very useful in other applications where the system is not as sensitive to basal leaky expression. This may be especially true in cases where expression of a given benign pathway enzyme is controlled by P_{esaR}, and certain levels of premature protein expression would not harm cell growth.

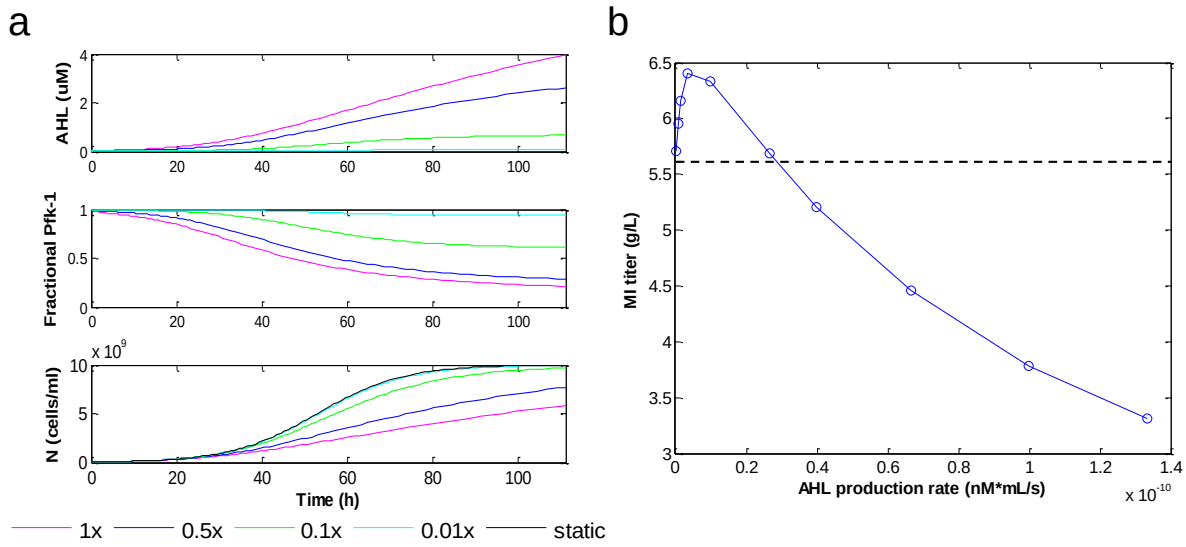

Supplementary Figure 1. Theoretical simulations of QS-based dynamic downregulation of Pfk-1 to ascertain expected trends in balancing growth and MI production from the G6P branchpoint. (a) A "1x" cellular AHL production rate was initially set to that used in You et al[4] (1.3 x 10-10 nM ml s^{-1}) and then varied accordingly. Lower AHL production rate leads to slower AHL accumulation and downregulation of Pfk-1 activity, and later growth arrest. The "static" trajectory refers to a strain without dynamic downregulation of Pfk-1. Fractional Pfk-1 denotes the Pfk-1 activity in the cell as a fraction of the basal levels without any downregulation. Kinetic parameters and rate equations are summarized in Supplementary Table 4. (b) Integration of the biomass and INO1 flux profiles over the batch time yielded expected endpoint MI titers for given AHL production rates. Titer profile shows an optimal AHL production rate to maximize titers, such that a very fast or very slow Pfk-1 knockdown is suboptimal. The dashed line indicates the corresponding expected MI titer from the "static" strain.

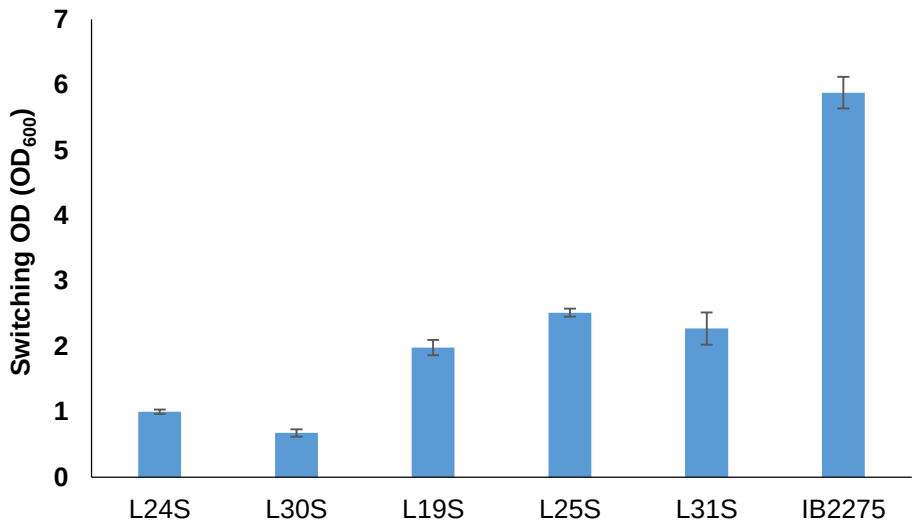

Supplementary Figure 2. Circuit switching ODs, determined through continuous measurement of plasmid-based GFP, in strains containing the QS-based valve controlling Pfk-1 expression. Strains containing the genomically-integrated QS-valve controlling Pfk-1 were transformed with pCOLA-P_{esaS}-GFP(LVA) and grown in MOPS medium with 10 g/L glucose. Switching OD was determined by ascertaining the cell density at the point of maximum fluorescence for a given strain. Constitutive GFP expression in the absence of EsaI (IB2275) was also tested to determine the basal GFP degradation kinetics without active arrest in transcription through a QS circuit. Trends for these switching ODs ascertained from continuous GFP measurement match those obtained from discrete measurements of Pfk-1 activity in Fig. 2C. Error represented as s.d. of triplicate cultures.

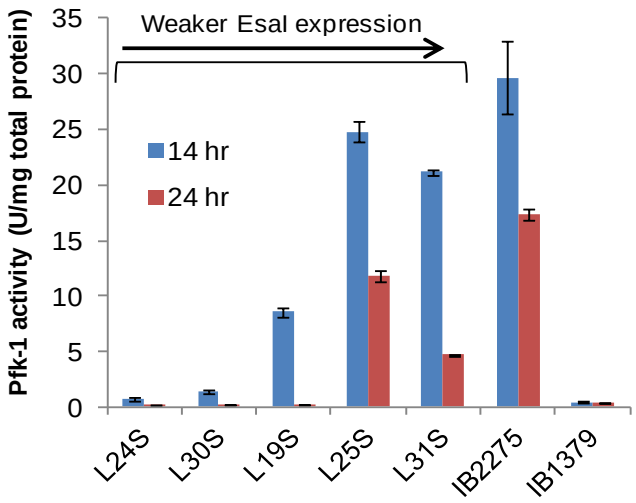

Pfk-1 activity (U/mg)	***L24S***	***L30S***	***L19S***	***L25S***	***L31S***	***IB2275***	***IB1379***
14 hrs	0.8 ± 0.1	1.4 ± 0.2	8.6 ± 0.4	24.8 ± 0.9	21.2 ± 0.3	29.7 ± 3.3	0.49 ± 0.02
24 hrs	0.16 ± 0.01	0.2 ± 0.0	0.26 ± 0.01	11.8 ± 0.5	4.7 ± 0.1	17.4 ± 0.5	0.35 ± 0.01
Final OD	7.82 ± 0.53	7.73 ± 0.26	8.34 ± 0.21	8.45 ± 0.11	8.59 ± 0.40	6.27 ± 0.52	8.08 ± 0.18

Supplementary Figure 3. Pfk-1 activity profiles and final ODs during MI production trials in MOPS medium with 10 g/L glucose for which the corresponding titers are given in Fig. 3A. The table shows the numerical values depicted in the plots. Error represented as s.d. of triplicate cultures.

a

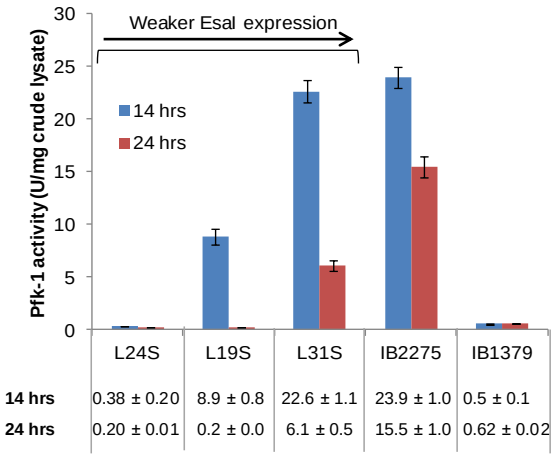

b

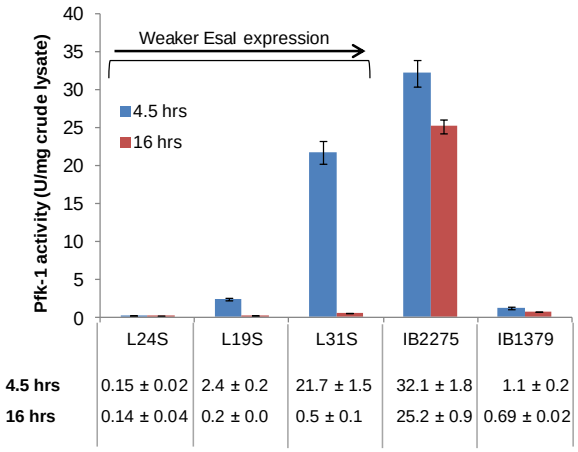

c

	L24S	L19S	L31S	IB2275	IB1379
Supplemented MOPS	10.08 ± 0.43	9.63 ± 0.97	9.83 ± 0.81	8.24 ± 0.79	9.40 ± 0.37
T12	11.25 ± 0.81	13.47 ± 0.64	8.62 ± 0.15	5.85 ± 0.15	9.02 ± 0.80

Supplementary Figure 4. Pfk-1 activity profiles during MI production trials in different growth media. (a) MOPS medium with 10 g/L glucose and 0.2% casamino acids. (b) T12 medium. Lower predicted expression of EsaI led to slower decline in Pfk-1 activity to below levels in IB1379. Trends in Pfk-1 activity profiles were similar across all medium compositions tested. Numbers below the plot represent the numerical value of the bars on the plot for clarity. (c) Final ODs in the cultures. Error represented as s.d. of triplicate cultures.

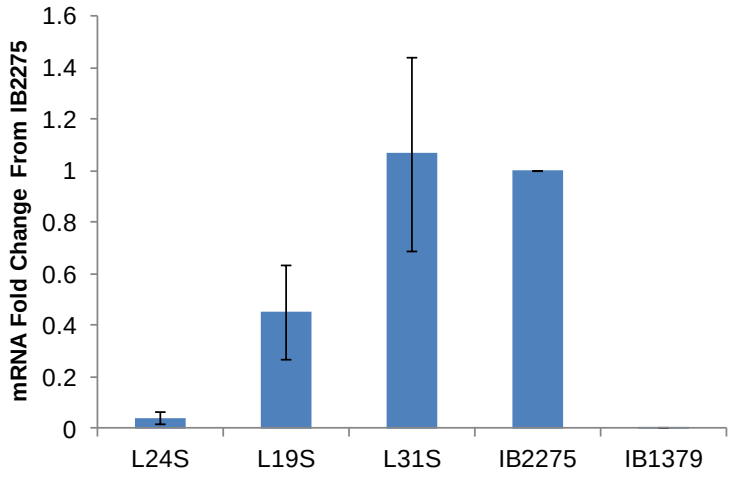

Supplementary Figure 5. mRNA levels from *pfkA* presented as a fold change from IB2275. Transcript levels corresponded to Pfk-1 activity trends (Supplementary Fig. 4A), confirming transcriptional regulation of Pfk-1. Error represented as s.d. of triplicate cultures.

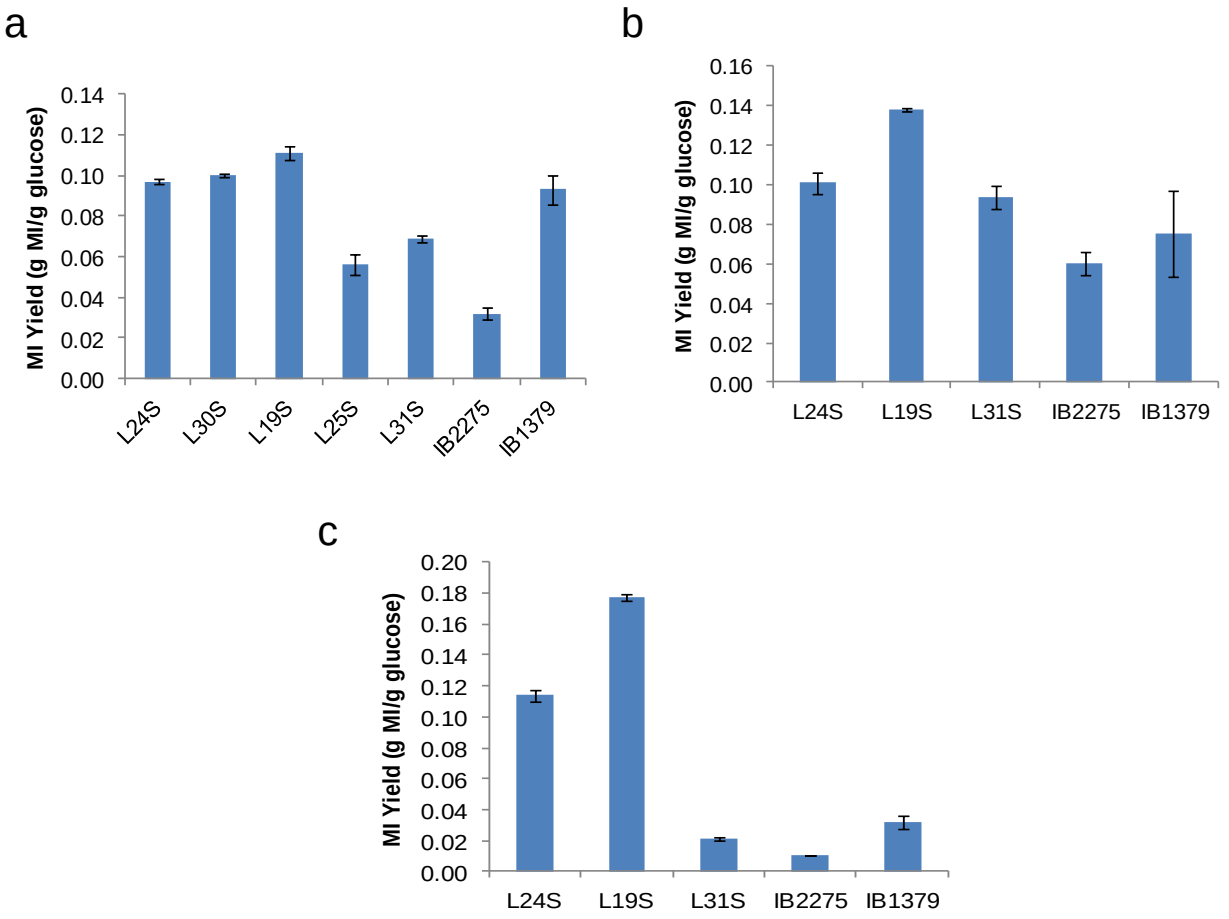

Supplementary Figure 6. Calculated yields of MI obtained in shake flask fermentations in different growth media. (a) MOPS minimal medium. (b) MOPS minimal medium supplemented with 0.2% casamino acids. (c) T12 medium. In all cases, the medium was supplemented with 10 g/L glucose. Absolute MI titers are provided in Fig. 3. Error reported as s.d. of triplicate cultures.

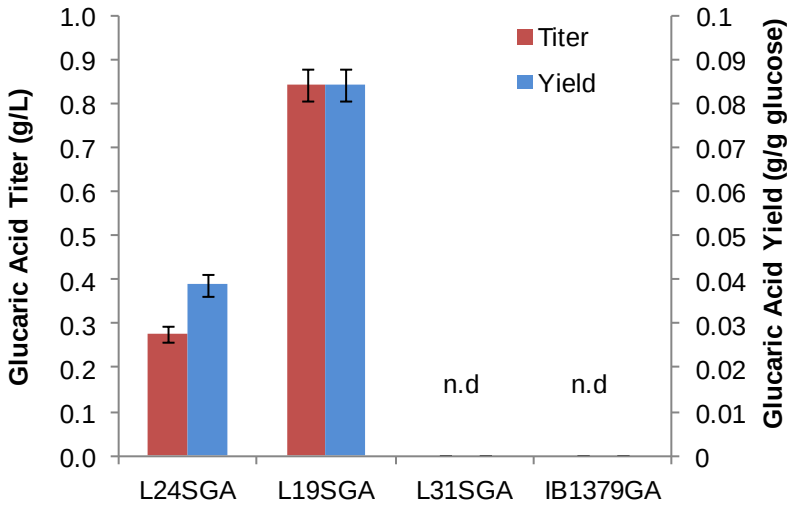

	L24SGA	L19SGA	L31SGA	IB1379GA
Final OD	5.94 ± 0.40	10.69 ± 1.01	7.03 ± 0.18	5.50 ± 0.74

Supplementary Figure 7. Glucaric acid titers and yields, and final culture ODs obtained in shake flask fermentations in T12 medium supplemented with 10 g/L glucose. n.d. denotes that titers that were below the detection limit. These titer data are also depicted in Fig. 4B. Error reported as s.d. of triplicate cultures.

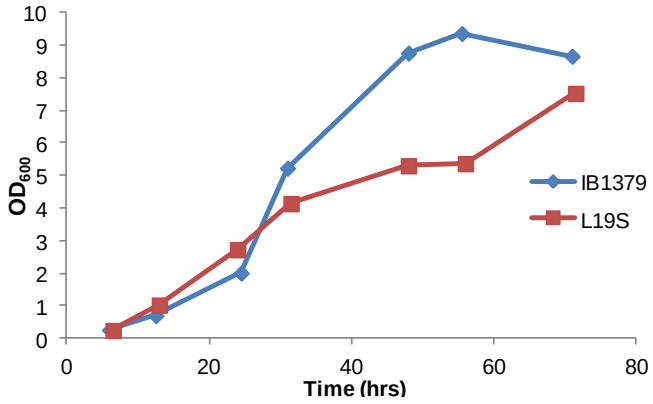

Strain	MI titer (g/L)	Final OD_{600}	Specific Titer (g MI / g DCW)	Yield (g MI/g glucose)
IB1379	0.56	8.7	0.14	0.056
L19S	1.19	7.5	0.34	0.119

Supplementary Figure 8. MI production in a 3L bioreactor in MOPS minimal medium supplemented with 10 g/L glucose. IB1379 reached a higher final OD_{600} than L19S but had more than 2-fold lower specific titer.

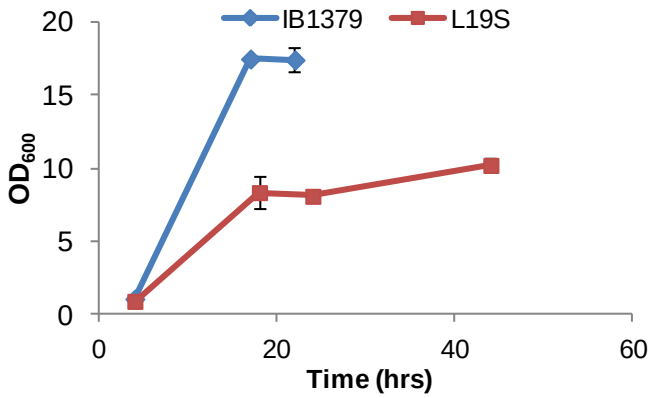

Strain	MI titer (g/L)	Final OD_{600}	Specific Titer (g MI/g DCW)	Yield (g MI/g glucose)
IB1379	0.23 ± 0.07	17.4 ± 0.8	0.03 ± 0.01	0.023 ± 0.007
L19S	1.28 ± 0.02	10.2 ± 0.5	0.27 ± 0.01	0.128 ± 0.002

Supplementary Figure 9. MI production in 3L bioreactors in T12 medium supplemented with 10 g/L glucose. Titers, specific titers and yields are the same as in Table 1. Error reported as s.d. of duplicate bioreactor runs.

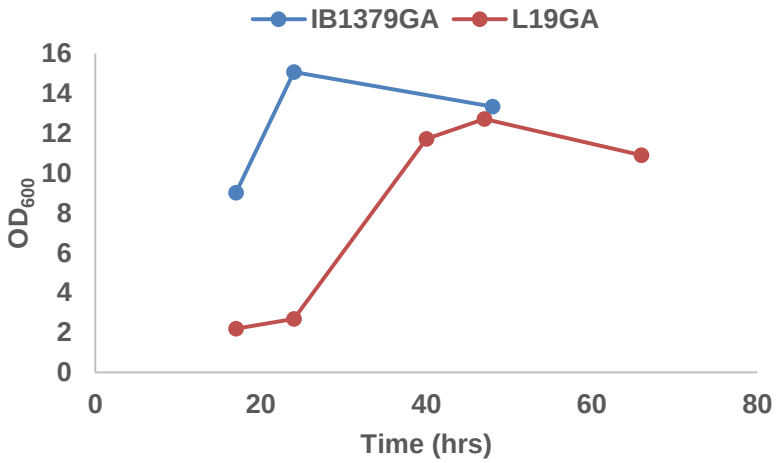

Strain	Glucaric Acid titer (g/L)	Final OD_{600}	Specific Titer (g MI/g DCW)	Yield (g MI/g glucose)
IB1379GA	0.17 ± 0.02	13.4 ± 0.7	0.03 ± 0.01	0.003 ± 0.001
L19GA	0.68 ± 0.11	10.5 ± 0.8	0.14 ± 0.01	0.014 ± 0.001

Supplementary Figure 10. Glucaric acid production in bioreactors in T12 medium supplemented with 10 g/L glucose. Titers, specific titers and yields are the same as in Table 1. Error reported as s.d. of duplicate bioreactor runs.

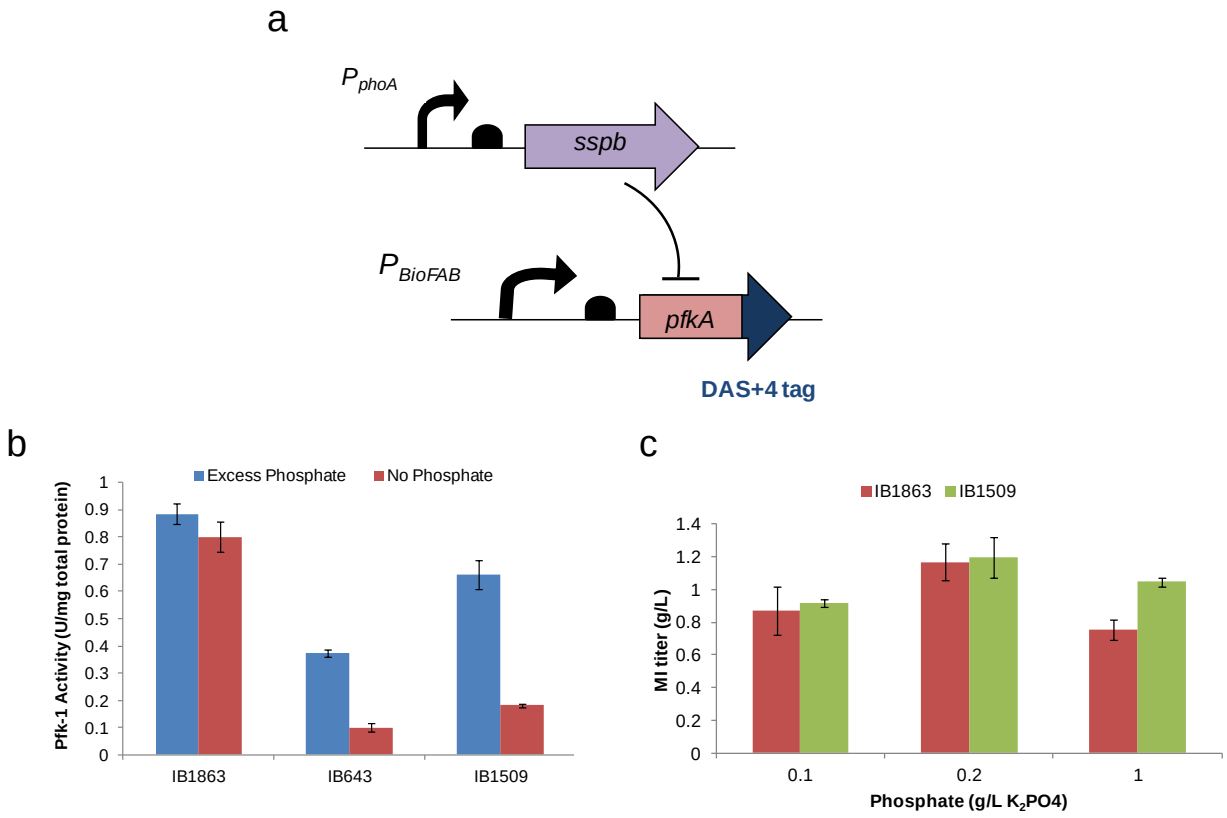

Supplementary Figure 11. Phosphate starvation-based control of *sspB* expression and Pfk-1 activity. (a) Schematic of the phosphate starvation-based circuit controlling *sspB* (b) IB643 and IB1509 contained identical strain backgrounds except for the strength of the constitutive promoter driving *pfkA* expression. Depletion of phosphate led to a decline in Pfk-1 activity in IB643 and IB1509. The latter was chosen for production trials as its basal activity in excess phosphate more closely matched the IB1863 control. (**c**) Production of MI with different initial phosphate levels. There was no significant difference in titers between IB1863 and IB1509. Both stains showed improved production at intermediate phosphate levels, compared to very low or excess phosphate. Error represented as s.d of triplicate trials.

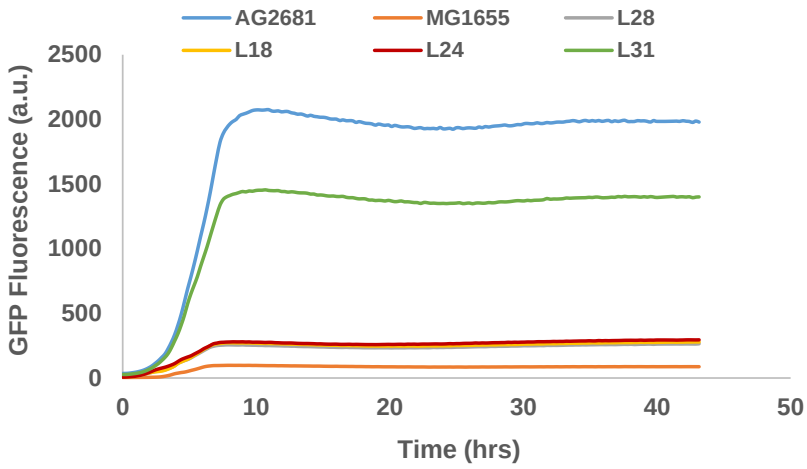

Supplementary Figure 12. Representative fluorescence profiles from QS-controlled expression of GFP without any appended degradation tag, in a subset of strains used for the initial circuit characterization in Fig. 1C. The plasmid pCOLA-P_{esaS}-GFP was inserted in a subset of strains from Fig. 1 to measure GFP depletion in the absence of an appended degradation tag, when its expression is dynamically downregulated by the QS circuit. Unlike in Fig. 1 where GFP is rapidly depleted due to the presence of the strong LVA tag, GFP pools remain relatively stable here after transcriptional arrest, illustrating the necessity of a degradation tag.

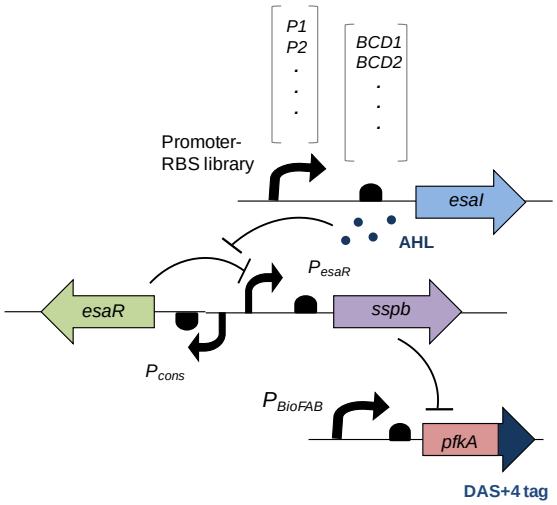

Supplementary Figure 13. Architecture of QS-based SspB-dependent regulation of Pfk-1 activity. Expression of EsaR was driven by a constitutive promoter and binds to P_{esaR} in the absence of AHL. The coding sequence of Pfk-1 is appended to a SspB-dependent SsrA degradation tag (DAS+4). EsaI expression was varied by instituting a library of promoters and RBS variants from Mutalik et al[14]. Production of AHL allowed EsaR to unbind from P_{esaR}, allow production of SspB which led to fast degradation of tagged Pfk-1. All components of the circuit were genomically integrated.

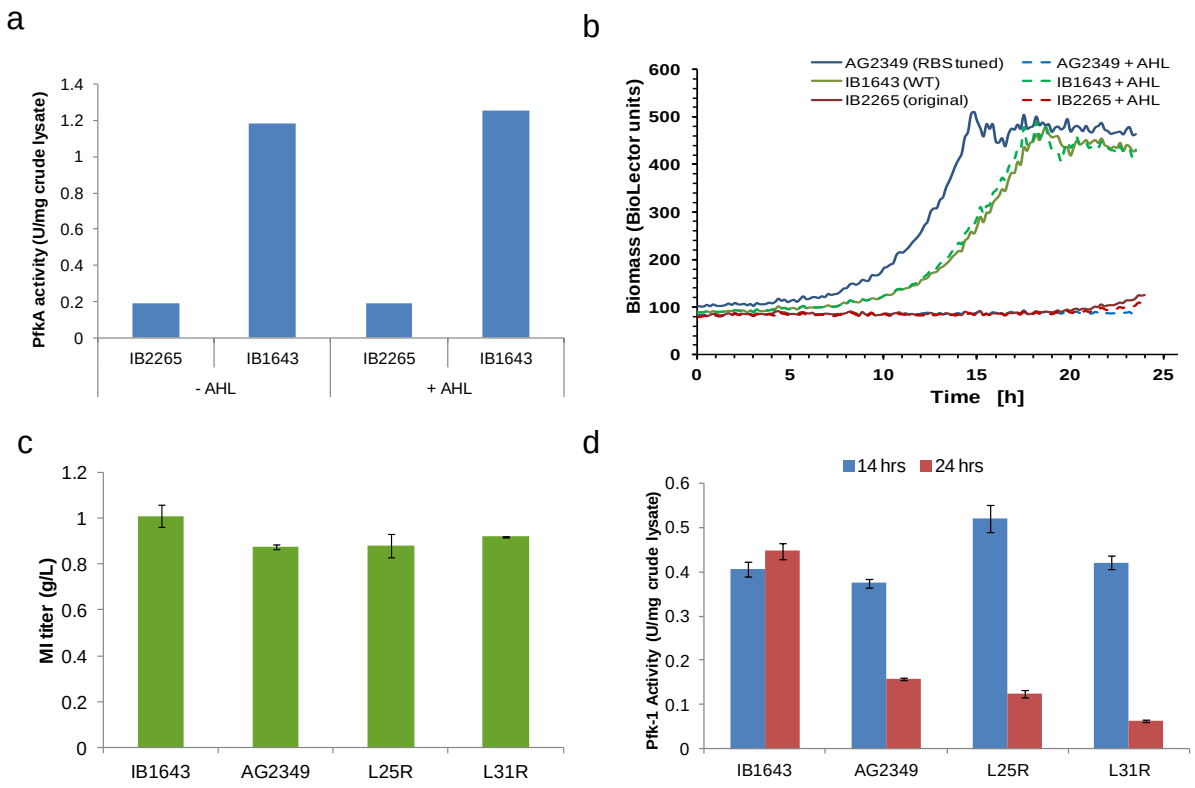

Supplementary Figure 14. Tuning and characterization studies for the QS-based SspB-dependent system for regulation of Pfk-1. (**a**) IB2265 showed no response to AHL as it already had lower Pfk-1 activity in crude lysates than the IB1643 control. (**b**) Growth profiles in minimal medium with glucose showed that IB2265 did not grow with or without AHL, suggesting that leaky SspB levels led to low Pfk-1 activity and growth defects. After tuning down the strength of its RBS to decrease leaky production of SspB, the strain responded to AHL. AG2349 grew only in the absence of AHL. (**c**) Constitutive expression of EsaI was instituted by integration of promoter and RBS variants. MI titers showed no boost over the IB1643 control. (**d**) Pfk-1 activity profiles during production studies showed that AG2349 (containing no EsaI expression cassette) still showed decline in activity over time. Error for (**c**) and (**d**) represented as s.d. of duplicate cultures.

Supplementary Table 1: All combinations of promoter and RBS variants constructed to yield a library of EsaI expression levels. Part numbers denote those registered in the BioFAB database. Predicted strengths of the combinations are represented as a percentage of the maximal strength found by Mutalik et al[14]. We were unable to integrate L2 and L17.

Promoter	RBS	Denotation	Predicted strength of *EsaI* expression[14]
apFAB95	apFAB682	L1	66.6
	apFAB683	L2	72.1
	apFAB690	L3	56.7
	apFAB693	L4	46.3
	apFAB699	L5	21.8
	apFAB700	L6	2.6
apFAB346	apFAB682	L8	75.3
	apFAB683	L9	53.5
	apFAB690	L10	41.8
	apFAB693	L11	33.6
	apFAB699	L12	15.8
	apFAB700	L13	2.2
apFAB296	apFAB682	L14	25.5
	apFAB683	L15	20.1
	apFAB690	L16	16.5
	apFAB693	L17	15.5
	apFAB699	L18	9.1
	apFAB700	L19	1.7
apFAB295	apFAB682	L20	12.9
	apFAB683	L21	9.8
	apFAB690	L22	8.7
	apFAB693	L23	7.8
	apFAB699	L24	4.8
	apFAB700	L25	1.3
apFAB65	apFAB682	L26	9.1
	apFAB683	L27	7.6
	apFAB690	L28	7.1
	apFAB693	L29	4.4
	apFAB699	L30	2.9
	apFAB700	L31	1.2

**** See Separate File for Supplementary Table 2 ****

**** See Separate File for Supplementary Table 2 ****

Supplementary Table 3: Summary of plasmids used in this study

Plasmid	Functional Genotype	Source
pCOLA-PesaS-GFP(LVA)	Tagged GFP under the P_{esaS} promoter in the pCOLA DUET vector	This study
pCOLA-PesaS-GFP	GFP under the P_{esaS} promoter in the pCOLA DUET vector	This study
pTrc-INO1	pTrc99A with *S. cerevisiae* INO1	[3]
pRSFD-IN-MI	INO1 (*S. cerevisiae*) and MIOX (*M. musculus*) under T7 promoter	[3]
pTrc-udh	Udh (*P. syringae*) expressed under the Trc promoter	[15]
pAC-EsaR	p15A; wildtype EsaR variant	[5]
pAC-EsaRI	p15A, EsaR and EsaI operon	[16]
pCS-P_{esaR}-lux	P_{esaR} inserted to drive *lux* operon	[5]
pCS-P_{esaS}-lux	P_{esaS} inserted to drive *lux* operon	[5]
pOSIP-KH	*attP* HK022, ccdB, HK022 integrase expressed by λ p_r under control of λ cI857	[17]
pOSIP-KO	*attP* 186, ccdB, 186 integrase expressed by λ p_r under control of λ cI857	[17]
pE-FLP	FLP recombinase expressed by *pE*	[17]
pCas9CR	Cas9 expression	[13]
pKDsgRNA-sspB	Guide RNA targeting 20-bp sequence of original *sspB* RBS; P_{arab} λ_γ λ_β λ_{exo}	[13], This study
pTKIP-neo	ColE1(pBR322)	[18]
pTKRED	*repA*101ts, araC, P_{lac} λ_γ λ_β λ_{exo}, *lacI*, P_{arab} - *1-Sce1*	[18]
pCP20	FLP recombinase expressed by λ p_r under control of λ cI857	CGSC #7629

Supplementary Table 4. Kinetic rate forms and parameter values utilized in the simulation of QS-based control of Pfk-1 activity.

Enzyme	Kinetic equation	Parameters	Value	Source
Pgi	Reversible Michaelis-Menten	$K_{M,Pgi,G6P}$	1.01	[19]
		$K_{M,Pgi,F6P}$	0.078	[19]
		K_{eq}	0.3	[20]
INO1	Irreversible two substrate Michaelis-Menten	$K_{M,Ino1,G6P}$	1.18	[21]
		$K_{M,Ino1,NAD}$	0.008	[22]
Pfk-I	Irreversible two substrate Michaelis-Menten	$K_{M,PfkA,F6P}$	0.03	[23]
		$K_{M,PfkA,ATP}$	0.06	[24]
N/A	N/A	k_{AHL}	1.3×10^{-10}	[4]
N/A	N/A	d_{AHL}	1.9×10^{-4}	[4]

Supplementary Table 5. Pfk-1 activity values presented in Fig. 2C. Error represented as s.d. of triplicate cultures.

	L24S	***L30S***	***L19S***	***L25S***	***L31S***	***IB2275***	***IB1379***
8.5 hrs	6.5 ± 1.9	2.4 ± 0.4	13.9 ± 0.7	19.4 ± 2.3	14.1 ± 1.1	28.2 ± 5.4	0.86 ± 0.04
14 hrs	0.28 ± 0.02	0.2 ± 0.0	0.33 ± 0.01	11.7 ± 1.9	4.6 ± 0.1	39.4 ± 3.0	0.86 ± 0.04
24 hrs	0.16 ± 0.03	0.19 ± 0.07	0.25 ± 0.04	0.24 ± 0.04	0.21 ± 0.01	28.2 ± 2.2	0.91 ± 0.08

**** See Separate File for Supplementary Table 6 ****

**** See Separate File for Supplementary Table 6 ****

References for Supplementary Information

1. Brockman, I. M. & Prather, K. L. J. Dynamic knockdown of E. coli central metabolism for redirecting fluxes of primary metabolites. *Metab. Eng.* **28,** 104–113 (2014).
2. Chassagnole, C., Noisommit-Rizzi, N., Schmid, J. W., Mauch, K. & Reuss, M. Dynamic modeling of the central carbon metabolism ofEscherichia coli. *Biotechnol. Bioeng.* **79,** 53–73 (2002).
3. Moon, T. S., Yoon, S.-H., Lanza, A. M., Roy-Mayhew, J. D. & Prather, K. L. J. Production of glucaric acid from a synthetic pathway in recombinant Escherichia coli. *Appl. Environ. Microbiol.* **75,** 589–95 (2009).
4. You, L., Cox, R. S., Weiss, R. & Arnold, F. H. Programmed population control by cell-cell communication and regulated killing. *Nature* **428,** 868–71 (2004).
5. Shong, J., Huang, Y.-M., Bystroff, C. & Collins, C. H. Directed evolution of the quorum-sensing regulator EsaR for increased signal sensitivity. *ACS Chem. Biol.* **8,** 789–95 (2013).
6. Shin, P. K. & Seo, J.-H. Analysis of E. coli phoA-lacZ Fudsion Gene Expression Inserted int a Multiopy Plasmid and Host Cell's Chromosome. *Biotechnol. Bioeng.* **36,** 1097–1104 (1990).
7. McGinness, K. E., Baker, T. a. & Sauer, R. T. Engineering Controllable Protein Degradation. *Mol. Cell* **22,** 701–707 (2006).
8. Johansson, L. *et al.* Shikimic acid production by a modified strain of E. coli (W3110.shik1) under phosphate-limited and carbon-limited conditions. *Biotechnol. Bioeng.* **92,** 541–552 (2005).
9. Youngquist, J. T., Rose, J. P. & Pfleger, B. F. Free fatty acid production in Escherichia coli under phosphate-limited conditions. *Appl. Microbiol. Biotechnol.* **97,** 5149–5159 (2013).
10. Ye, Q. *et al.* High-level production of heterologous proteins using untreated cane molasses and corn steep liquor in Escherichia coli medium. *Appl. Microbiol. Biotechnol.* **87,** 517–525 (2010).
11. Agarwal, L., Isar, J., Dutt, K. & Saxena, R. K. Statistical optimization for succinic acid production from E. coli in a cost-effective medium. *Appl. Biochem. Biotechnol.* **142,** 158–167 (2007).
12. Salis, H. M. The ribosome binding site calculator. *Methods Enzymol.* **498,** 19–42 (2011).
13. Reisch, C. R. & Prather, K. L. J. The no-SCAR (Scarless Cas9 Assisted Recombineering) system for genome editing in Escherichia coli. *Sci. Rep.* (2015).
14. Mutalik, V. K. *et al.* Precise and reliable gene expression via standard transcription and translation initiation elements. *Nat. Methods* **10,** 354–60 (2013).
15. Yoon, S.-H., Moon, T. S., Iranpour, P., Lanza, a. M. & Prather, K. J. Cloning and Characterization of Uronate Dehydrogenases from Two Pseudomonads and Agrobacterium tumefaciens Strain C58. *J. Bacteriol.* **191,** 1565–1573 (2009).
16. Shong, J. & Collins, C. H. Engineering the esaR promoter for tunable quorum sensing- dependent gene expression. *ACS Synth. Biol.* **2,** 568–75 (2013).
17. St-Pierre, F. *et al.* One-step cloning and chromosomal integration of DNA. *ACS Synth. Biol.* **2,** 537–541 (2013).
18. Kuhlman, T. E. & Cox, E. C. Site-specific chromosomal integration of large synthetic constructs. *Nucleic Acids Res.* **38,** (2010).
19. Ogawa, T., Mori, H., Tomita, M. & Yoshino, M. Inhibitory effect of phosphoenolpyruvate on glycolytic enzymes in Escherichia coli. *Res. Microbiol.* **158,** 159–163 (2007).
20. Ishii, N. *et al.* Multiple High-Throughput Analyses Monitor the Response of E. coli to Perturbations. *Science (80-.).* **316,** 593–597 (2007).

21. Majumder, A. L., Johnson, M. D. & Henry, S. a. 1L-myo-Inositol-1-phosphate synthase. *Biochim. Biophys. Acta - Lipids Lipid Metab.* **1348,** 245–256 (1997).

22. Balleza, E. *et al.* Regulation by transcription factors in bacteria: Beyond description. *FEMS Microbiol. Rev.* **33,** 133–151 (2009).

23. Bergert, S. a & Evans, P. R. Steady-State Fluorescence of. *Society* 8477–8480 (1991).

24. Blangy, D., Buc, H. & Monod, J. Kinetics of the allosteric interactions of phosphofructokinase from Escherichia coli. *J. Mol. Biol.* **31,** 13–35 (1968).